WIND-WAVE SURFACE TURBULENCE AND LANGMUIR CIRCULATIONS ON THE UPPER MIXED LAYER OF MARINE ECOSYSTEMS

Mahmoud Moussa
Laboratoire hydraulique, Ecole Nationale d'Ingénieurs de Tunis
B.P. 37, le Belvédère, 1002 Tunis, Tunisia

Philippe Maurel
Institut de Mécanique des Fluides de Toulouse, UMR 5502
Allée Camille Soula, 31400 Toulouse, France

Lucien Masbernat
Institut de Mécanique des Fluides de Toulouse, UMR 5502
Allée Camille Soula, 31400 Toulouse, France

ABSTRACT

We present an experimental and numerical analysis of wind-generated currents and turbulence in the sea surface layer. We examine laboratory and field data in order to define a new characterisation of the turbulent scales at the interface. The numerical study concerns the development of 2-D vertical model, formulated in (U, ψ, Ω, k, ε) variables. This model allows to predict the average and turbulent kinematics fields and takes into account the wave-current-turbulence interactions that maintain the Langmuir circulation and increase the turbulence level under wind waves.

1 . INTRODUCTION

The dynamics of the surface layer of the ocean and transfers through the top meters of water are significantly affected by interactions between wind-generated waves, wind-induced mean current and turbulence. Field and laboratory experiments show two main characteristics of wind-wavy shear surface, the first is related to the surplus of Turbulent Kinetic Energy (TKE) produced beneath the air-water interface by breaking, and the second concerns the mean wind-driven current and wave field interactions, which is responsible for the Langmuir circulations (organised longitudinal roll-vortex structures beneath the water surfaces under water-waves forcing) mechanism. These two main characteristics were investigated separately by various authors.

The most interesting field measurements on Lake Ontario, presented and analysed by Kitaigorodskii et al. (1983), and Terray et al. (1996), indicate that the level of both turbulent kinetic energy and its dissipation rate were considerably increased with respect to usual shear flows. On the other hand, many experimental studies, carried out in laboratory tanks by Cheung and Street (1988), and Thais and Magnaudet (1996), describe the structure of both orbital and turbulent motions below wind water waves. They pointed the relative importance of the orbital fluctuations on the total motion scales. Another set of laboratory experiences were carried out at the Toulouse Fluid Mechanics Institute (IMFT)'s wind-wave tunnel, where turbulent characteristics and mean velocity fields were measured (Magnaudet and Thais, 1995 ; Prodhomme, 1988).

The first theoretical explanation about Langmuir circulations existence was obtained by Craik and Leibovich (1976). They were able to calculate explicitly the wave-mean current interactions which maintain the cellular motions. Moreover, these mechanisms were explored by Magnaudet and Masbernat (1990); these authors developed a new theoretical analysis with non constant eddy viscosity, showing the character of wave-turbulence interactions.

In this paper we present a new model to predict the three dimensional mean current and turbulence under wind-waves forcing. It takes into account the wave-current-turbulence interactions which maintain the Langmuir circulation and increase the turbulence level at the upper mixed layer. This work is based on experimental and numerical analysis of wind-generated currents and turbulence in the sea surface layer. We define a new characterisation of the turbulence scales at the interface which were used in the numerical model.

2 . ANALYSIS OF EXPERIMENTAL DATA

In the experimental analysis, we examine laboratory and field data in order to estimate the turbulent kinetic energy and the turbulent dissipation rate at the air-sea interface. The first set of laboratory experiences we analyse, are due to Prodhomme (1988) and Magnaudet and Thais (1995). They are carried out at the IMFT's wind-wave tunnel (Toulouse). This tunnel has a test section of 1.2 m large and 2 m high. The turbulent characteristics and mean velocity fields were measured at a fetch of about 14 m and with 1 m depth of water (Moussa, 1999). The wind velocity varied from 6.7 m/s to 13.5 m/s. The water flows are 26 ℓ/s (Prodhomme, 1988) and 20 ℓ/s (Magnaudet and Thais, 1995).

The second set of laboratory experiences was carried out by Thais and Magnaudet (1996) at the IMST's wind-wave tunnel (Marseille). Measurements of the turbulent characteristics and mean velocity fields were collected at a 26 m of fetch, with 0.9 m of water depth, without water flow and on the channel axis. A triple decomposition of the fluctuating motion was used to distinguish potential and rotational parts of the orbital motion, as well as turbulent fluctuations. In these experiences, the wind velocities are 5.9 m/s and 7.8 m/s.

The last experimental data used here are obtained from experiments carried out at the Lake Ontario by Terray et al. (1996). The measurements of the turbulent dissipation rate are collected from a fixed tower installed in 12.5 m depth of water and 1100 m from the western end of the lake. The wind speed varied from 7.01 m/s to 12.05 m/s.

In order to estimate the turbulent kinetic energy, k, and the turbulent dissipation rate, ε, at the air-sea interface, we suppose beneath this region, as confirmed by many works, the existence of an energy balance dominated by a diffusion-dissipation equilibrium. So the transport equation of TKE of a (k, ε) simplified 1-D vertical (z) turbulence model is :

$$\frac{d}{dz}\left(C_\mu \frac{k^2}{\varepsilon} \frac{dk}{dz} \right) = \varepsilon \qquad (1)$$

The solution of equation (1), gives an exponential vertical decrease of the turbulence from the interface :

$$k = k_I \exp\left[\sqrt{\frac{2}{3\,C_\mu}} \frac{\varepsilon_I}{k_I^{3/2}} z \right]$$

and

$$\varepsilon = \varepsilon_I \exp\left[\sqrt{\frac{3}{2\,C_\mu}} \frac{\varepsilon_I}{k_I^{3/2}} z \right] \qquad (2)$$

where k_I and ε_I are the turbulent characteristics at the interface and z the ascendant vertical co-ordinate with z=0 at the interface (C_μ=0.09). These solutions are agree with experimental results (figure 1), at least on the interfacial region, and allow us to determine the interfacial values of k_I and ε_I. The solutions (2) give also an eddy viscosity which decreases exponentially with the depth from the interfacial eddy viscosity.

If we put on the same graph (figure 2) these interfacial turbulent characteristics, we obtain the non-dimensional following laws :

$$k_I / u_{*I}^2 = 5.2\left(gX / u_{*g}^2 \right)^{1/6}$$

and

$$\varepsilon_I / g\,u_{*I} = 0.315\left(gX / u_{*g}^2 \right)^{-5/12} \qquad (3)$$

where X is the fetch, u_{*_I} and u_{*g} are water and gas friction velocities deduced from the interfacial wind stress τ_I ($u_{*_I}=\sqrt{\tau_I / \rho}$, ρ is the water density, and $u_{*g}=\sqrt{\tau_I / \rho_g}$, ρ_g is the gas density). Expressions (3) reproduce the high level of both turbulent kinetic energy and its dissipation rate, compared to the usual values on the shear flows, produced beneath the air-water interface by waves breaking. We note that the TKE at the interface, k_I, deduced from (3) is a part of the wave energy at the interface.

3 . THE MODEL EQUATIONS

The numerical study concerns the development of a model allowing to predict the 3-D mean velocity components and turbulent kinematic fields. We consider a study flows, full developed in the longitudinal (x) direction. In the spanwise (y) direction the computed domain corresponds to two symmetric contra-rotating Langmuir circulations. The model is formulated in (U, ψ, Ω) variables, where U is the streamwise mean velocity, ψ is the stream function and Ω is the longitudinal vorticity. In the longitudinal vorticity equation, we introduce the orbital vorticity term S_Ω, which generates Langmuir circulations. This term is expressed according to Craik and Leibovich (1976) formulation :

$$S_\Omega = -\frac{dU_S}{dz}\frac{\partial U}{\partial y} \quad (4)$$

where U_S is the wave Stokes drift. The three mean velocity components U, V, W represent the downwind (x-longitudinal axis), crosswind (y-horizontal spanwise axis, origin situated at channel axis) and vertical velocities (z-vertical axis, upward from surface origin). All cases treated are steady, homogeneous in density and fully developed in longitudinal direction; the secondary cells will be placed at (y-z) plane. The eddy viscosity is predetermined by a two equations (k-ε) turbulence model.

The model is formulated in non dimensional form by using characteristics scales; the length scale is the inverse of the wave number K^{-1} , the velocity scales are u_{*I} and u_o that represent a part of the wave energy defined by: $u_o = \delta^{0.5} (gK)^{0.5} a$ (a is the wave amplitude, and $\delta = aK$ is the wave steepness). *If the dimensional variables were marked by " ^ ", the non dimensional ones were defined as:*

$$(x, y, z) = (K\hat{x}, K\hat{y}, K\hat{z}) \quad (5)$$

$$(U, V, W) = \left(\frac{\hat{U} - <\hat{U}>}{u_{*I}^2 / u_o}, \frac{\hat{V}}{\delta^{0.25} u_{*I}}, \frac{\hat{W}}{\delta^{0.25} u_{*I}}\right) \quad (6)$$

$$k = \frac{\hat{k}}{u_o^2} \; ; \; \varepsilon = \frac{\hat{\varepsilon}}{K u_o^3} \quad \text{and} \quad \nu_t = C_\mu \frac{k^2}{\varepsilon} = \frac{K\hat{\nu}_t}{u_o} \quad (7)$$

Where $<\hat{U}>$ is the average water flow in the channel. The reference scales used in expressions (5) to (7) allows a good assemblage of experimental dataset. The reference eddy viscosity deduced from (7) is: $\nu_{to} = u_o / K$. The reference scales introduced in (5) and (6) are comparable to that defined by Leibovich (1977) in witch the constant eddy viscosity is here replaced by ν_{to}.

According to (5), (6) and (7), the equations of the model may be written as follows:

$$V\frac{\partial U}{\partial y} + W\frac{\partial U}{\partial z} = L_a\left[\frac{\partial}{\partial y}\left(\nu_t \frac{\partial U}{\partial y}\right) + \frac{\partial}{\partial z}\left(\nu_t \frac{\partial U}{\partial z}\right) + \frac{J^*}{Kh}\right] \quad (8)$$

$$V\frac{\partial \Omega}{\partial y} + W\frac{\partial \Omega}{\partial z} = L_a\left[\frac{\partial}{\partial y}\left(\nu_t \frac{\partial \Omega}{\partial y}\right) + \frac{\partial}{\partial z}\left(\nu_t \frac{\partial \Omega}{\partial z}\right)\right] - \frac{\partial U_S}{\partial z}\frac{\partial U}{\partial y} \quad (9)$$

$$\frac{\partial^2 \psi}{\partial y^2} + \frac{\partial^2 \psi}{\partial z^2} = -\Omega \quad (10)$$

with : $V = \psi_{,z}$; $W = -\psi_{,y}$; $\Omega = W_{,y} - V_{,z}$

$$V\frac{\partial k}{\partial y} + W\frac{\partial k}{\partial z} = L_a\left[\frac{\partial}{\partial y}\left(\frac{\nu_t}{\sigma_k}\frac{\partial k}{\partial y}\right) + \frac{\partial}{\partial z}\left(\frac{\nu_t}{\sigma_k}\frac{\partial k}{\partial z}\right) + P_{rod} - \varepsilon\right] \quad (11)$$

$$V\frac{\partial \varepsilon}{\partial y} + W\frac{\partial \varepsilon}{\partial z} = L_a\left[\begin{array}{c}\frac{\partial}{\partial y}\left(\frac{\nu_t}{\sigma_\varepsilon}\frac{\partial \varepsilon}{\partial y}\right) + \frac{\partial}{\partial z}\left(\frac{\nu_t}{\sigma_\varepsilon}\frac{\partial \varepsilon}{\partial z}\right) \\ + C_{\varepsilon 1} P_{rod}\frac{\varepsilon}{k} - C_{\varepsilon 2}\frac{\varepsilon^2}{k}\end{array}\right] \quad (12)$$

$$\text{and: } P_{rod} = L_a^{-2}\nu_t\left[\begin{array}{c}\delta^{-1}L_a^{-2}\left(\left(\frac{\partial U}{\partial y}\right)^2 + \left(\frac{\partial U}{\partial z}\right)^2\right) \\ + \left(2\left(\frac{\partial V}{\partial y}\right)^2 + 2\left(\frac{\partial W}{\partial z}\right)^2 + \left(\frac{\partial V}{\partial z} + \frac{\partial W}{\partial y}\right)^2\right)\end{array}\right] \quad (13)$$

Where h is the depth of water, J^* is the average non dimensional longitudinal pressure gradient, U_S is the Stokes drift, with monochromatic waves in deep water $U_S(z) = \exp(2z)$, and L_a is a new Langmuir number that appears correlated to the Froude number: $L_a = u_o / (\delta^{0.5} u_{*I})$. This number is first introduced by Leibovich (1977) but the eddy viscosity is here replaced by ν_{to}. In the equations (11) and (12), C_μ, σ_k, σ_ε, $C_{\varepsilon 1}$ and $C_{\varepsilon 2}$ (= 0.09; 1.0; 1.3; 1.65; 1.92) are the constants of the (k-ε) turbulence model.

These equations were completed by boundary conditions. We impose, at the interface, the longitudinal mean velocity from the shear stress due to the wind:

$$\nu_t U_{,z}(y, 0) = 1 \text{ and } \Omega_{,z}(y, 0) = \psi(y, 0) = 0 \quad (14)$$

For the turbulence model, the boundary conditions at the interface are defined by the expressions (3) issued from the experimental analysis presented above. At the bottom, we assume the classical wall boundary conditions. Simulations were performed adopting an integration domain that corresponds to the width (2L) of each experimental channel. Symmetrical boundary conditions were imposed at each lateral side of the domain (y= −KL and y= KL).

A finite difference approach was used, and an implicit scheme was employed for the resolution of the equations (8) to (12) with discretization of the domain into equally spaced mesh. The numerical convergence is controlled by minimal global imposed error criteria.

4 . SIMULATIONS RESULTS

The model is employed to the simulation of laboratories conditions (Thais and Magnaudet, 1996 ; Magnaudet and Thais, 1995 ; Prodhomme, 1988) with Langmuir circulations. Figure 3 shows examples of three profiles of vertical mean velocity (W) computed in the case wind velocity 11.65 m/s. The model results were compared with experimental data from Prodhomme (1988) on three verticals, which are situated at the channel axis, at 30 cm and 53 cm to the axis (marked by **00**, **30**, **and 53** respectively). The model reproduces correctly the intensity of the secondary flows. Two contra-rotating cells were generated in the cross-sections of the channel, and the difference between the downwelling and upwelling velocities shows cells asymmetry.

One of the most important affects of the secondary flows are shown in figure 4 which represents the vertical profiles of the non-dimensional turbulent shear stress ($-\overline{u'w'} / u_{*I}^2$) referred to the wind speed 11.65 m/s case (Prodhomme, 1988): the profiles are non linear as in the case of parallel flows. Figure 5 shows the experimental vertical profiles of the TKE compared with the model results. The turbulent characteristics computed by the model are in good order of experimental ones. The longitudinal mean velocity graphic (figure 6) shows the same orders of magnitude for the measured and calculated values.

Figures 3, 4 and 5 show the evident differences between a Langmuir circulations presence flow (measured and calculated) and that parallel situation simulated by the model. These figures indicate the importance of the convection transport consequence, by secondary motions, on the different results. The importance of the interfacial conditions and the convection transport by Langmuir circulations were observed on the balance of the TKE transport. Figure 7 shows an example of the TKE balance on the channel axis, in the case wind velocity 7.8 m/s (Prodhomme, 1988). The contribution of the diffusion and the convection under water waves are very important. In fact, below the interfacial region dominated by a diffusion-dissipation equilibrium, the energy balance are controlled by the convection and the diffusion: in this region, the diffusion as well as the convection values reach 3 or 4 times as big as the dissipation rate.

Furthermore, The model is used to simulate the case of parallel flow in Lake Ontario. Figure 8 shows the vertical of turbulent dissipation rate computed under wind velocity 11 m/s. These numerical results are compared to experimental data from Terray et al. (1996).

The comparison of the numerical results either in laboratories experiences or in fields flows, with or without Langmuir circulations, confirms the pertinence of the improvements proposed (3) to represent the interfacial conditions.

REFERENCES

Cheung, T. K., and Street, R. L., 1988, "The turbulent layer in the water at an air-water interface", *J. Fluid Mech.*, Vol. 194, pp. 133-151.

Craik, A. D. D., and Leibovich, S., 1976, "A rational model for Langmuir circulations", *J. Fluid Mech.*, Vol. 73, pp. 401-426.

Kitaigorodskii, S. A., Donelan, M. A., Lumley, J. L., and Terray, E. A., 1983, "Wave-turbulence interactions in the upper ocean. Part II", *J. Phys. Oceanogr.*, Vol. 13, pp. 1988-1999.

Leibovich, S., 1977, "On the evolution of system of wind drift currents and Langmuir circulations in the ocean. Part 1: Theory and averaged current", *J. Fluid Mech.*, Vol. 79, pp. 715-743.

Magnaudet, J., and Thaïs, L., 1995, "A triple decomposition of the fluctuating motion below laboratory wind water waves", *J. Geophys. Res.*, Vol. 100, N° C1, pp. 741-771.

Magnaudet, J., and Masbernat, L., 1990, "Interactions des vagues de vent avec le courant moyen et la turbulence", *C. R. Acad. Sci. Paris*, t. 311, Série II, pp. 1461-1466.

Moussa, M., 1999, "Turbulence et circulation générées par le vent dans les eaux de surface", *Thèse de Doctorat d'Etat., Ecole Nat. Ing. de Tunis*, Tunisia, 196 p.

Prodhomme, M. T., 1988, "Turbulence sous les vagues de vent", *Thèse de Doctorat, Inst. Nat. Polytech. de Toulouse*, France, 231 p.

Terray, E. A., Donelan, M. A., Agrawal, W. M., Drennan, W. M., Kahma, K. K., Williams III, A. J., Hwang, P. A., and Kitaigorodskii, S. A., 1996, "Estimates of kinetic energy dissipation under breaking waves", *J. Phys. Oceanogr.*, Vol. 26, pp. 792-807.

Thaïs, L., and Magnaudet, J., 1996, "Turbulent structure beneath surface gravity waves sheared by the wind", *J. Fluid Mech.*, Vol. 328, pp. 313-344.

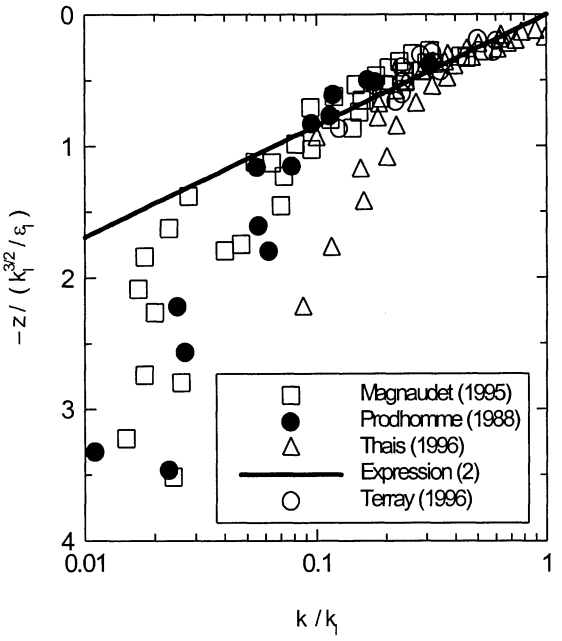

Figure 1. *Vertical TKE profiles.*

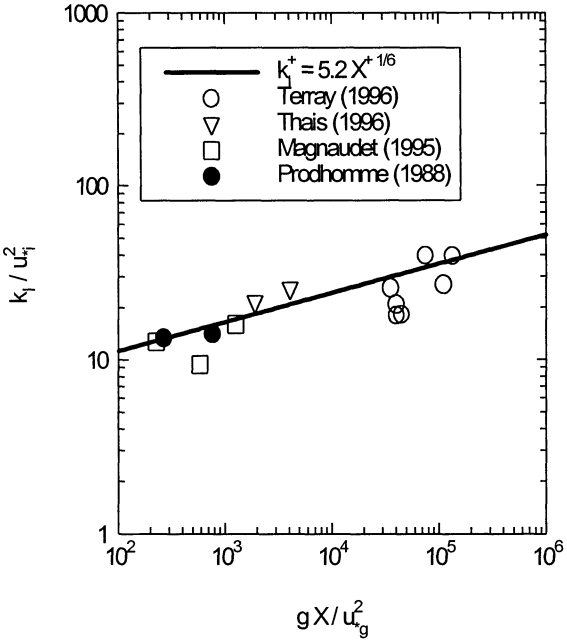

Figure 2. *Interfacial TKE as a function of the fetch.*

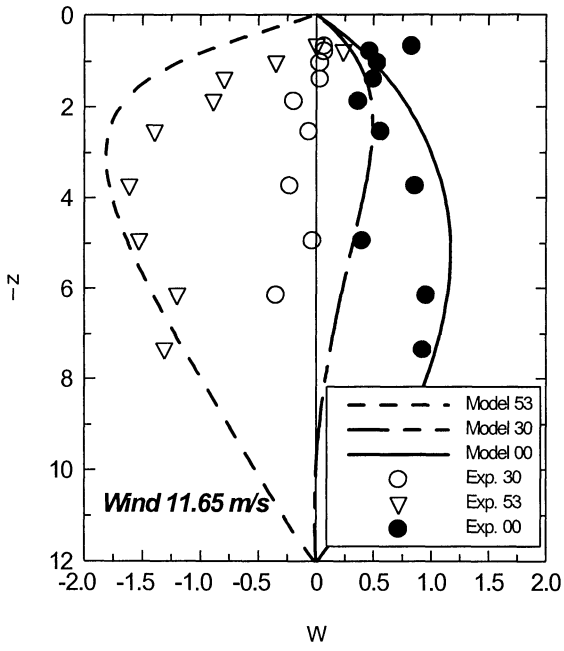

Figure 3. *Profiles of non dimensional W, case wind velocity 11.65 m/s.*

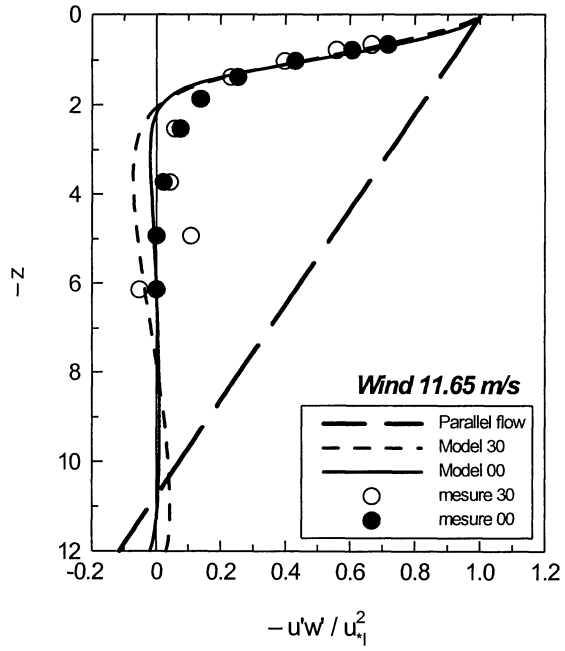

Figure 4. *Profiles of turbulent shear stress, case wind velocity 11.65 m/s.*

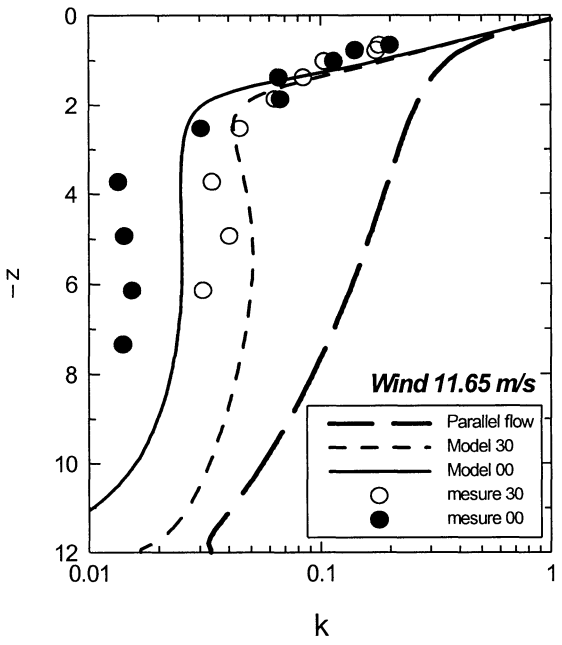

Figure 5. *Profiles of non dimensional TKE, case wind velocity 11.65 m/s.*

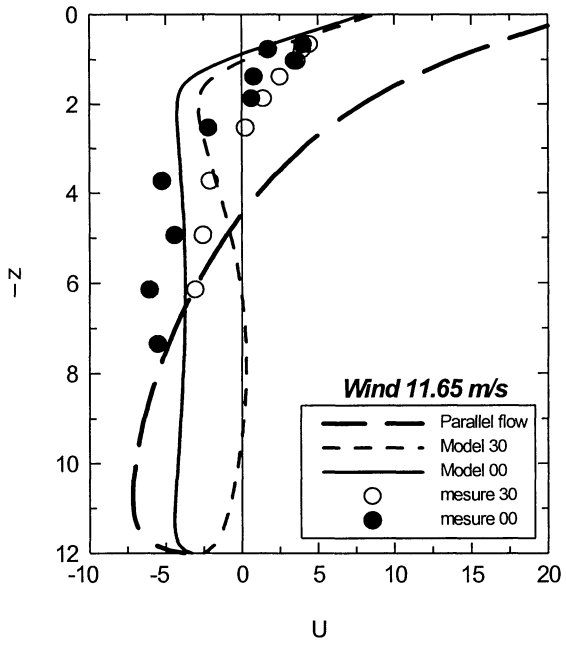

Figure 6. *Profiles of non dimensional U, case wind velocity 11.65 m/s.*

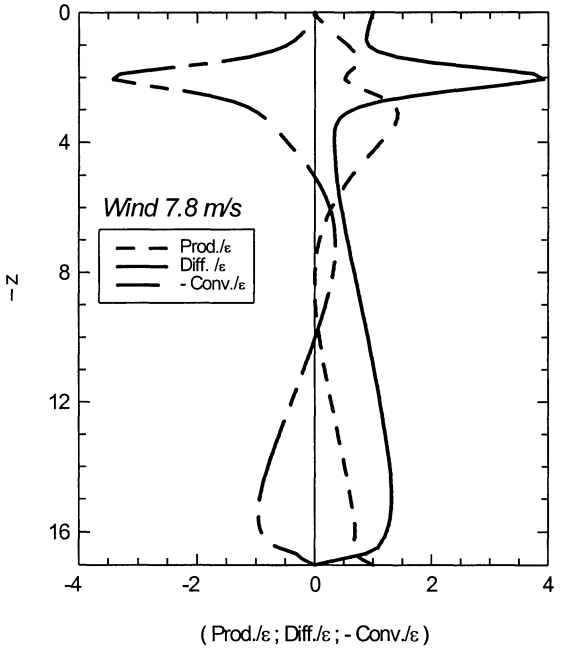

Figure 7. *TKE balance on the channel axis, case wind velocity 7.8 m/s.*

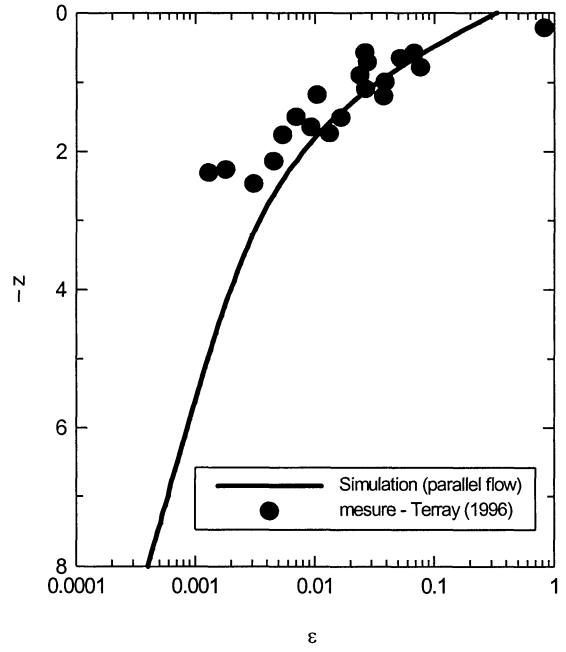

Figure 8. *Vertical ε profile, case wind velocity ≈ 11m/s.*